Lorenz equations

In 1963 Ed Lorenz published a paper titled *"Deterministic non-periodic flows"* in the Journal of Atmospheric Sciences in which he studied an idealization of a hydrodynamical system represented by a fluid layer between two free surfaces. The system is sketched in Figure 1.

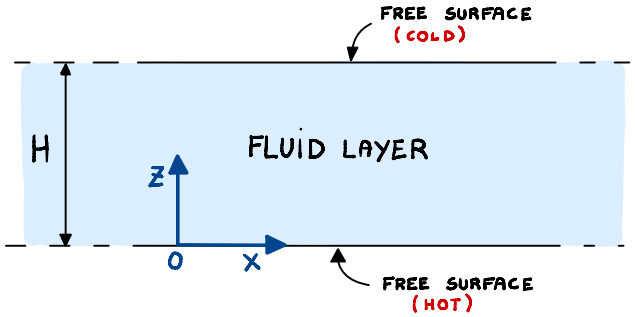

Figure 1: Fluid layer between two free surfaces. The "free surface" boundary conditions are defined by setting vertical component of the fluid velocity v_z equal zero at $z = 0$ and $z = H$ (Dirichlet boundary conditions), and the derivative of the horizontal component with respect to the vertical axis $\partial v_x/\partial z$ equal to zero at $z = 0$ and $z = H$ (Neumann boundary conditions). The free surfaces are kept at constant temperature T_{hot} (bottom surface) and $T_{\text{cold}} \leq T_{\text{hot}}$ (top surface).

The equations of motion for this system are[1]

$$\begin{cases} \dfrac{\partial \nabla^2 \Psi}{\partial t} + \dfrac{\partial \Psi}{\partial z}\dfrac{\partial}{\partial x}\nabla^2\Psi - \dfrac{\partial \Psi}{\partial x}\dfrac{\partial}{\partial z}\nabla^2\Psi = \nu \nabla^4 \Psi + g\beta \dfrac{\partial \theta}{\partial x}, \\ \dfrac{\partial \theta}{\partial t} + \dfrac{\partial \Psi}{\partial z}\dfrac{\partial \theta}{\partial x} - \dfrac{\partial \Psi}{\partial x}\dfrac{\partial \theta}{\partial z} = \kappa \nabla^2 \theta + \dfrac{\Delta T}{H}\dfrac{\partial \Psi}{\partial x}, \end{cases} \tag{1}$$

where $\Psi(x, z, t)$ is the streamfunction that defines the fluid velocity components as

$$v_x(x, z, t) = \frac{\partial \Psi(x, z, t)}{\partial z}, \qquad v_z(x, z, t) = -\frac{\partial \Psi(x, z, t)}{\partial x}, \tag{2}$$

$\theta(x, z, t)$ represents the deviation of the temperature distribution in the fluid layer from the pure thermal conduction state, i.e.,

$$\theta(x, z, t) = T(x, z, t) - \left(\frac{\Delta T}{H} z\right), \tag{3}$$

$\Delta T = T_{\text{hot}} - T_{\text{cold}}$ is the temperature difference between the isothermal horizonal fluid layers at $z = 0$ (hot) and $z = H$ (cold), H is the depth of the fluid layer, and g, β, ν and κ are, respectively, the acceleration of gravity, the isobaric compressibility, the kinematic viscosity, and the thermal diffusivity of the fluid. When studying natural convection problems it is convenient to define the following dimensionless number

$$Ra = \frac{g\beta H^3 \Delta T}{\nu \kappa} \qquad \text{(Rayleigh number)} \tag{4}$$

which represents the relative importance between the effects of the buoyancy forces due to temperature differences, and the effects of the viscosity forces.

[1]The model equations (1) are called Oberbeck-Boussinesq approximation of the natural convection problem. The first equation in (1) is the Navier-Stokes equation written in a 2D streamfunction-vorticity formulation. The second equation is the Fourier equation governing the the propagation of temperature within the fluid layer due to diffusion and transport by the fluid velocity.

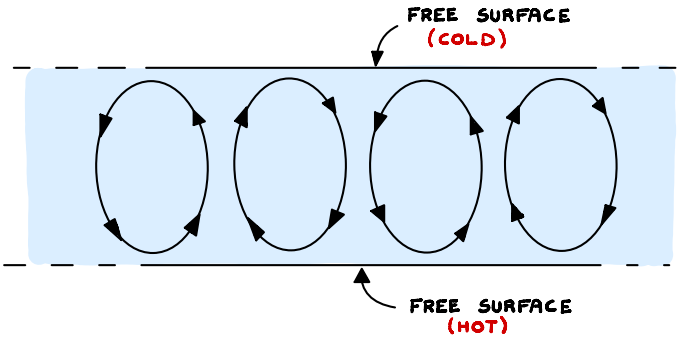

Figure 2: One-roll convection patterns arising in the infinite fluid layer system sketched in Figure 1. The convection patter is generated for Rayleigh numbers Ra slightly above the critical one $Ra_c = 657.5$ (onset of convective instability).

Intuitively, when the buoyancy forces exceed some threshold depending on thermal diffusivity and viscosity the fluid then the system transitions from a state of pure thermal conduction to natural convection, with an infinite number of one-roll patterns as shown in Figure 2. The critical Rayleigh number that characterizes the transition point between thermal condition and natural convection is called *onset of convective instability*. For the system sketched in Figure 1 the critical Rayleigh number can be computed analytically as

$$Ra_c = \frac{27\pi^4}{4} = 657.5. \tag{5}$$

For $Ra < Ra_c$ the fluid does not move, while for Ra slightly above Ra_c we have an infinite number of one-roll convection patterns (see Figure 2). The system transitions from the no-flow state to the one-roll convection pattern state via a *supercritical pitchfork bifurcation*. By expanding θ and Ψ in (1) in a double Fourier series as and projecting onto the Fourier basis it is possible to transform (1) into a finite-dimensional nonlinear system of differential equations for the time-dependent functions (Fourier coefficients) representing the coefficients of the expansion.

In certain cases, all except three Fourier coefficients eventually tend to zero, and those three modes undergo irregular non-periodic fluctuations. Lorenz observed that the same solutions would have been obtained if the Fourier series had at the start been truncated to include a total number of three terms. Accordingly, he looked for time-dependent solutions of (1) in the form

$$\Psi(x,z,t) = 3\kappa X(t) \sin\left(\frac{\pi}{\sqrt{2}H}x\right)\sin\left(\frac{\pi}{H}z\right), \tag{6}$$

$$\theta(x,z,t) = \frac{\Delta T Ra_c}{\pi Ra}\left[\sqrt{2}Y(t)\cos\left(\frac{\pi}{\sqrt{2}H}x\right)\sin\left(\frac{\pi}{H}z\right) - Z(t)\sin\left(\frac{2\pi}{H}z\right)\right], \tag{7}$$

where $X(t)$, $Y(t)$ and $Z(t)$ are the Fourier coefficients (functions of time alone). By substituting (6)-(7) into (1) and omitting trigonometric terms other that those occurring in (6)-(7) we obtain

$$\begin{cases} \dot{X} = -\sigma X + \sigma Y \\ \dot{Y} = rX - Y - XZ \qquad \text{(Lorenz system)} \\ \dot{Z} = XY - bZ \end{cases} \tag{8}$$

In ODE system above, the time derivative is with respect to the dimensionless time

$$\tau = \frac{3\pi^2\kappa}{2H^2}t, \tag{9}$$

and the parameters r, σ and b are defined as

$$\begin{cases} r = \dfrac{Ra}{Ra_c} & \text{(relative Rayleigh number)} \\ \sigma = \dfrac{\nu}{\kappa} & \text{(Prandtl number)} \\ b = \dfrac{8}{3} \end{cases} \tag{10}$$

The system of equations (6)-(8) represents a simplified solution to the natural convection equations (1). In fact, with $X(t)$, $Y(t)$ and $Z(t)$ available from (8) we can then reconstruct the velocity and temperature fields within the fluid layer by using (6) and(7).

Properties of the Lorenz system. The Lorenz system is a three-dimensional nonlinear dynamical system with quadratic polynomial non-linearities. Additionally, it possesses the following fundamental properties.

- **Symmetry.** The transformation $(X, Y) \to (-X, -Y)$ leaves the system (8) invariant. This implies that the phase portrait is symmetric with respect to the Z-axis. As a consequence, trajectories with initial condition on Z-axis stay on the Z-axis for all times. This can be also seen by noting that the initial condition $(0, 0, Z_0)$ yields a trajectory described by the system $\dot{X} = 0$, $\dot{Y} = 0$, $\dot{Z} = -bZ$.

- **Volume contraction.** The volume of any compact region $D(t) \subset \mathbb{R}^3$ advected by the flow of any three dimensional system evolves in time as (see Theorem 2 in Appendix A)

$$\frac{dV(t)}{dt} = \int_{D(t)} \nabla \cdot \boldsymbol{f}(\boldsymbol{x}) d\boldsymbol{x}. \tag{11}$$

  The divergence of vector field at the right hand side of the Lorenz system (8) is

$$\begin{aligned} \nabla \cdot \boldsymbol{f} =& \frac{\partial f_1}{\partial X} + \frac{\partial f_2}{\partial Y} + \frac{\partial f_3}{\partial Z} \\ =& \frac{\partial}{\partial X}(-\sigma X + \sigma Y) + \frac{\partial}{\partial Y}(rX - Y - XZ) + \frac{\partial}{\partial Z}(XY - bZ) \\ =& -(\sigma + b + 1). \end{aligned} \tag{12}$$

  Recalling that σ and b are positive numbers we see that $\nabla \cdot \boldsymbol{f} < 0$ at each point in phase space. By substituting (12) into (11) we obtain

$$\frac{dV(t)}{dt} = -(\sigma + b + 1) \int_{D(t)} 1 d\boldsymbol{x} = -(\sigma + b + 1) V(t), \tag{13}$$

  i.e

$$V(t) = V(0) e^{-(\sigma + b + 1)t}. \tag{14}$$

  Hence, the volume of *any* compact region advected by the flow generated by (8) shrinks to zero exponentially fast in time, independently of where we pick the region, or its initial shape.

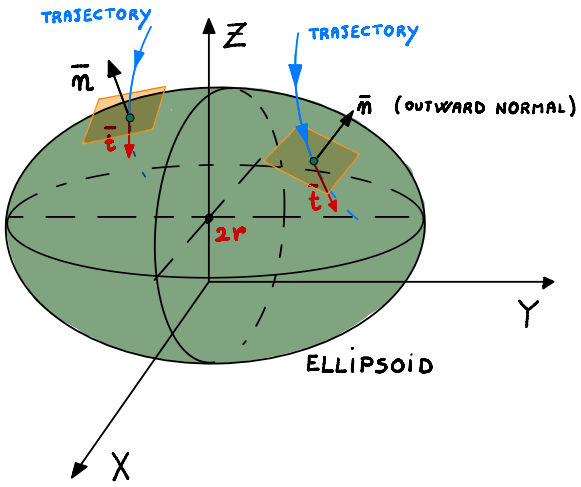

Figure 3: Trajectories of the Lorenz system do not escape the ellipsoid (15) if Q is chosen large enough.

- **Trajectories are bounded.** Consider the ellipsoid

$$E(Q) = \{(x, y, z) \in \mathbb{R}^3 : rx^2 + \sigma y^2 + \sigma(z - 2r)^2 = Q\}, \tag{15}$$

where Q is a positive number representing how big the ellipsoid is[2]. The outward normal to the surface of the ellipsoid is (see Figure 3)

$$\boldsymbol{n} = (2rx, 2\sigma y, 2\sigma(z - 2r)) \tag{18}$$

and it coincides with the components of the gradient of

$$F(x, y, z) = rx^2 + \sigma y^2 + \sigma(z - 2r) - Q \tag{19}$$

evaluated at the zero level set of F. The tangent vector to an arbitrary trajectory intersecting the surface of the ellipsoid (15) at a point $(x_e, y_e, z_e) \in E(Q)$ is given by the right hand side of (8) evaluated at (x_e, y_e, z_e), i.e.,

$$\boldsymbol{t} = (-\sigma x_e + \sigma y_e, rx_e - y_e - x_e z_e, x_e y_e - bz_e)\,. \tag{20}$$

Taking the dot product between the outward normal vector (18) and the vector tangent to a trajectory passing through an arbitrary point on the ellipsoid (15) yields

$$\begin{aligned} \boldsymbol{n} \cdot \boldsymbol{t} =& 2rx_e(-\sigma x_e + \sigma y_e) + 2\sigma y_e(rx_e - y_e - x_e z_e) + 2\sigma(z_e - 2r)(x_e y_e - bz_e) \\ =& -2\sigma\left(rx_e^2 + y_e^2 + b(z_e - r)^2 - br^2\right). \end{aligned} \tag{21}$$

Clearly, if

$$rx_e^2 + y_e^2 + b(z_e - r)^2 > br^2, \tag{22}$$

[2]Note that the ellipsoid (15) is centered at $(x, y, z) = (0, 0, 2r)$ and it can be written as

$$\frac{x^2}{Q/r} + \frac{y^2}{Q/\sigma} + \frac{(z - 2r)^2}{Q/\sigma} = 1. \tag{16}$$

In this form we see that the semi-axes are

$$a_1 = \sqrt{\frac{Q}{r}}, \qquad a_2 = \sqrt{\frac{Q}{\sigma}}, \qquad a_3 = \sqrt{\frac{Q}{\sigma}}. \tag{17}$$

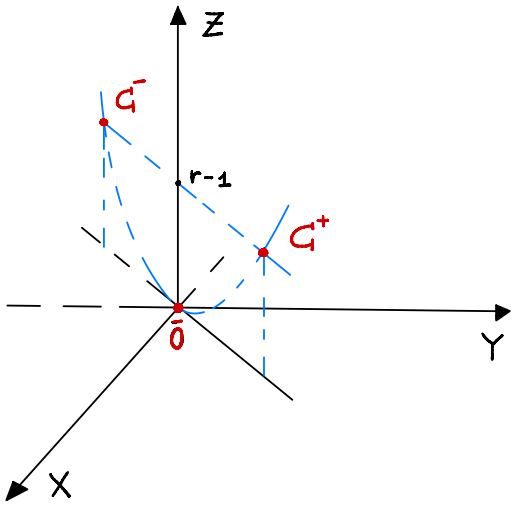

Figure 4: Fixed points of the Lorenz system for $r > 1$.

then $\boldsymbol{n} \cdot \boldsymbol{t} < 0$, i.e., the vector tangent to the trajectory intersecting the surface of the ellipsoid points inward. Of course, if Q in (15) is sufficiently large, then all points on the surface of the ellipsoid $E(Q)$ will satisfy condition (22). This proves that the ellipsoid itself will serve as the boundary for the trajectories corresponding to any initial condition on its surface or inside it.

Stability analysis of fixed points. The nullclines of (8) are

$$\begin{cases} X = Y \\ Y = rX - XZ \\ Z = \dfrac{XY}{b} \end{cases} \tag{23}$$

Substituting last equation into the second and taking the first into account yields

$$X - rX + \frac{X^3}{b} = 0 \quad \Rightarrow \quad X\left(1 - r + \frac{X^2}{b}\right) = 0 \quad \Rightarrow \quad \begin{cases} X^* = 0 \\ X^* = \pm\sqrt{b(r-1)} \end{cases} \tag{24}$$

By Substituting this back into (23) we obtain the following three fixed points:

$$(0,0,0) \qquad \text{for all } r \tag{25}$$

and

$$\boldsymbol{C}^{\pm} = \left(\pm\sqrt{b(r-1)}, \pm\sqrt{b(r-1)}, r-1\right) \qquad \text{for } r > 1. \tag{26}$$

These fixed points shown in Figure 4 for $r > 1$. The stability of the fixed points is determined by the eigenvalues of the Jacobian matrix

$$\boldsymbol{J_f}(X,Y,Z) = \begin{bmatrix} -\sigma & \sigma & 0 \\ r - Z & -1 & -X \\ Y & X & -b \end{bmatrix} \tag{27}$$

evaluated at $(X^*, Y^*, Z^*) = (0,0,0)$ and $(X^*, Y^*, Z^*) = \boldsymbol{C}^{\pm}$.

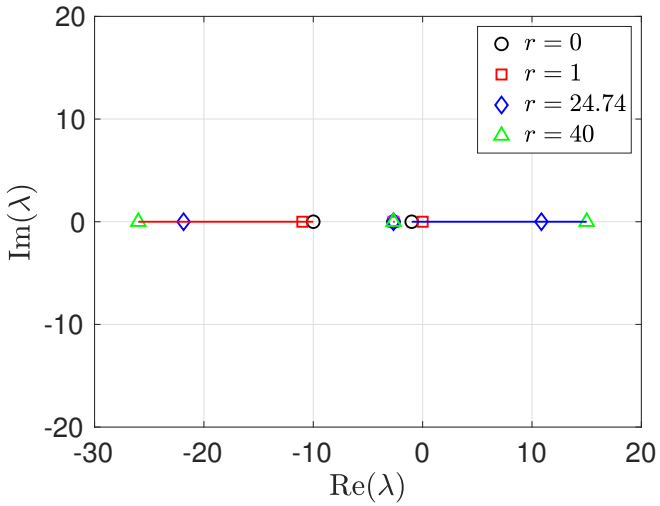

Figure 5: Stability analysis of the origin. Shown are eigenvalues of the Jacobian matrix (28) as a function of r for $b = 8/3$ and $\sigma = 10$. The origin undergoes a zero-eigenvalue bifurcation (supercritical pitchfork) for $r = 1$.

- **Stability analysis of the origin.** Evaluating the Jacobian (27) at $(X^*, Y^*, Z^*) = (0, 0, 0)$ yields

$$\boldsymbol{J_f}(0,0,0) = \begin{bmatrix} -\sigma & \sigma & 0 \\ r & -1 & 0 \\ 0 & 0 & -b \end{bmatrix} \tag{28}$$

The eigenvalues are the roots of the third-order characteristic polynomial

$$p(\lambda) = \det\left(\boldsymbol{J_f} - \lambda \boldsymbol{I}\right) = -(b+\lambda)\left[(\sigma+\lambda)(1+\lambda) - r\sigma\right], \tag{29}$$

i.e.,

$$\lambda_{1,2} = \frac{-(\sigma+1) \pm \sqrt{(\sigma+1)^2 - 4\sigma(1-r)}}{2}, \qquad \lambda_3 = -b. \tag{30}$$

It is easy to show that all eigenvalues are real[3] for each r (see Figure 5).

Specifically,

a) For $r < 1$ we have that $\lambda_{1,2,3} < 0$, i.e., the origin is a stable node. Such stable node is *globally attracting*, i.e., it attracts all trajectories disregarding where the initial condition is.

b) For $r = 1$ we have that $\lambda_{2,3} < 0$, and $\lambda_1 = 0$, i.e., the origin is a non-hyperbolic fixed point. For $r = 1$ the Jacobian (28) has one zero eigenvalue, i.e., the system undergoes a *zero-eigenvalue bifurcation*. Using Sotomayor's Theorem 6 in course note 9, it can be shown that such bifurcation is a *supercritical pitchfork bifurcation* representing the onset of convective instability of the fluid layer (note that for $r = 1$ we have $Ra = Ra_c$ in (10)). Such bifurcation generates three fixed point for $r \geq 1$, i.e., the origin (which becomes a 3D saddle node) and two stable nodes $\boldsymbol{C}^{\pm}$.

c) For $r > 1$ we have that $\lambda_{2,3} < 0$, and $\lambda_1 > 0$, i.e., the origin is a three-dimensional saddle node with two stable manifolds and one unstable manifold. The eigenvectors corresponding to $\lambda_1 < 0$ and $\lambda_2 > 0$ lie in the (X, Y)-plane, while the eigenvector corresponding to $\lambda_3 = -b < 0$ lies on the Z-axis.

[3]Note that the smallest value of the quantity within the square root in $\lambda_{1,2}$ defined in (30) is positive. In fact, such value is achieved for $r = 0$ and can be written as

$$(\sigma+1)^2 - 4\sigma = (\sigma-1)^2 > 0. \tag{31}$$

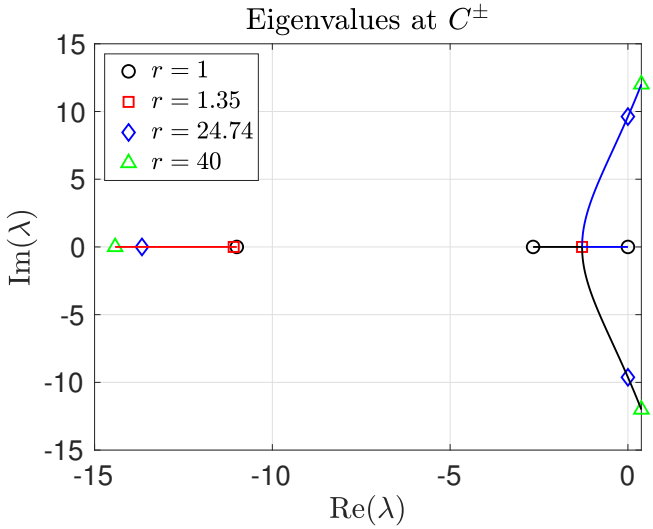

Figure 6: Stability analysis of $\boldsymbol{C}^{\pm}$. Shown are eigenvalues of the Jacobian matrix (32) as a function of r for $b = 8/3$ and $\sigma = 10$. The fixed points $\boldsymbol{C}^{\pm}$ undergo a *subcritical Hopf* bifurcation for $r = 24.74$.

- **Stability analysis of $\boldsymbol{C}^{\pm}$.** Evaluating the Jacobian (27) at $(X^*, Y^*, Z^*) = \boldsymbol{C}^{\pm}$ yields

$$\boldsymbol{J_f}\left(\boldsymbol{C}^{\pm}\right) = \begin{bmatrix} -\sigma & \sigma & 0 \\ 1 & -1 & \mp\sqrt{b(r-1)} \\ \pm\sqrt{b(r-1)} & \pm\sqrt{b(r-1)} & -b \end{bmatrix} \tag{32}$$

The eigenvalues of $\boldsymbol{J_f}(\boldsymbol{C}^{\pm})$ are roots of the characteristic polynomial

$$p(\lambda) = \det\left(\boldsymbol{J_f} - \lambda \boldsymbol{I}\right) = -(\sigma+\lambda)\left[(1+\lambda)(b+\lambda) + b(r-1)\right] + \sigma\left[(b+\lambda) - b(r-1)\right], \tag{33}$$

i.e.,

$$\lambda^3 + (\sigma + b + 1)\lambda^2 + (r+\sigma)b\lambda + 2b\sigma(r-1) = 0. \tag{34}$$

In Figure 6 we plot the eigenvalues of (32), i.e., the roots of (34), as a function of r. We see that

a) For $1 < r \leq 1.35$ the fixed points $C^{\pm}$ are stable nodes.

b) For $1.35 < r < 24.74$ the fixed points $C^{\pm}$ are still stable but there exist two complex conjugate eigenvalues with negative real part. The real Jordan form of (32) allow us to identify a plane on which the local dynamics around $\boldsymbol{C}^{\pm}$ is equivalent to a stable spiral (see Figure 7 in the course note 4).

c) For $r = 24.74$ both fixed points $C^{\pm}$ undergo a *subcritical Hopf bifurcation*. To identify the value of r at which such Hopf bifurcation occurs we set $\lambda = \omega i$ in (34), i.e.,

$$-i\omega^3 - (\sigma + b + 1)\omega^2 + i(r+\sigma)b\omega + 2b\sigma(r-1) = 0. \tag{35}$$

In other words, we look for the value of r that yields an imaginary eigenvalue. Setting the real and the imaginary parts of the complex number at the left hand side of (35) equal to zero yields, respectively,

$$\omega^2 = \frac{2b\sigma(r-1)}{\sigma + b + 1}, \qquad \omega^2 = (r+\sigma)b. \tag{36}$$

By substituting ω^2 from one equation into the other we obtain

$$r_H = \sigma\frac{\sigma + b + 3}{\sigma - (b+1)}. \tag{37}$$

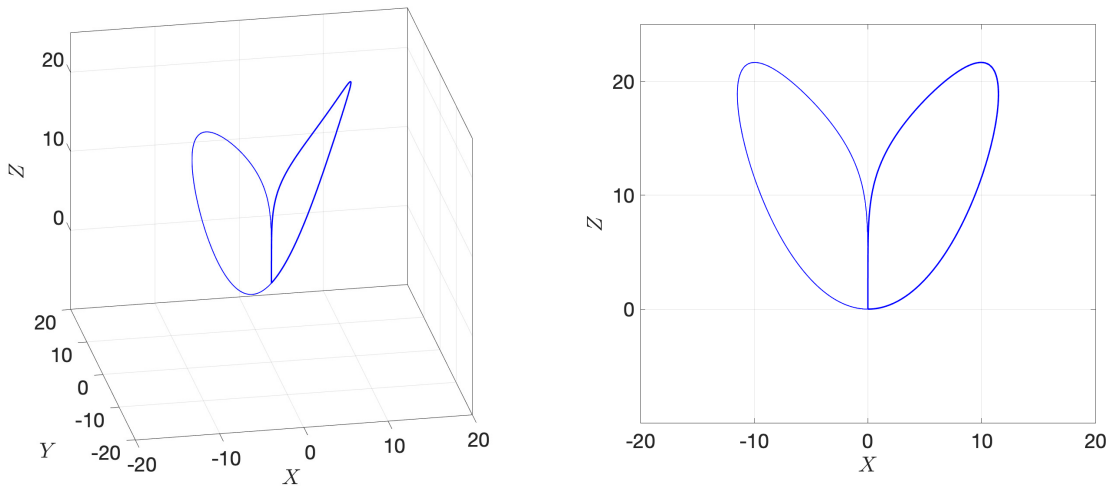

Figure 7: Homoclinic butterfly for $r = 13.92655741$, $\sigma = 10$ and $b = 8/3$. For $r > 13.92655741$ a complicated set is created at the origin of the system via a process called "homoclinic explosion". This process is described, e.g., in the book *"The Lorenz Equations: Bifurcations, Chaos,and Strange Attractors"*, by Colin Sparrow (Springer 1984). The set arising form the homoclinic explosion can yield *transient chaos* (see Figure 8).

This is the critical value of the relative Rayleigh number r at which the subcritical Hopf bifurcation occurs. For $\sigma = 10$ and $b = 8/3$ (37) yields $r_H = 24.74$ (see Figure 6).

d) For $r > 24.74$ the fixed points $\boldsymbol{C}^{\pm}$ are unstable spirals in 3D, with a stable manifold of dimension 1 (we have a one-dimensional eigenspace corresponding to a negative eigenvalue).

Summary of the bifurcation analysis of equilibria. Let us provide a brief summary of our findings related to the stability analysis of the fixed points as a function of the relative Rayleigh number r.

- For $r < 1$ there is only one fixed point at the origin (stable node) and it is globally attracting.
- For $r = 1$ the origin is non-hyperbolic (but still a stable node). The origin undergoes a supercritical pitchfork bifurcation, which yields two new fixed points $\boldsymbol{C}^{\pm}$.
- For $1 < r < r_H$ the origin is unstable (3D saddle node with a one-dimensional unstable manifold) while $\boldsymbol{C}^{\pm}$ turn from stable nodes to 3D stable spirals. Such transition happens at $r = 1.35$ for $\sigma = 10$ and $b = 8/3$. As r approaches r_H from the left, two unstable limit cycles approach the stable spirals at $\boldsymbol{C}^{\pm}$.
- For $r = r_H$ both fixed points $\boldsymbol{C}^{\pm}$ undergo a subcritical Hopf bifurcation in which the unstable cycles mentioned above are created and exist for $r < r_H$. As we reduce r below r_H, the two unstable cycles become bigger and bigger and they eventually end up touching each other at the origin for $r^* = 13.92655741$, creating the so-called *homoclinc butterfly* shown in Figure 7. For $r > r^*$ a complicated set is created at the origin via a bifurcation process called "homoclinic explosion". This process is described, e.g., in the book *"The Lorenz Equations: Bifurcations, Chaos, and Strange Attractors"*, by Colin Sparrow (Springer 1984). The set arising form the homoclinic explosion can yield *transient chaotic trajectories*, as shown in Figure 8.
- For $r > r_H$ the fixed points $\boldsymbol{C}^{\pm}$ are both three-dimensional unstable spirals. Both spirals have a one-dimensional stable manifold.

Hence, for $r > r_H$ there are no stable fixed points as both the origin and $\boldsymbol{C}^{\pm}$ are unstable. However, we

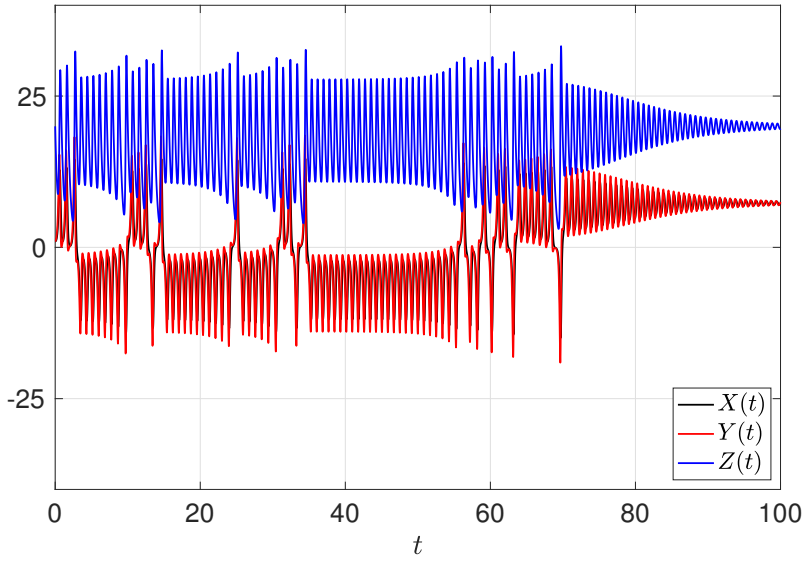

Figure 8: Transient chaos for $r = 20$, $\sigma = 10$ and $b = 8/3$. Note that for $t > 75$ the trajectory is spiraling towards $\boldsymbol{C}^+$ and will eventually get there in an infinite time.

have seen that volumes in the phase space shrinks to zero asymptotically fast in time. Moreover, there exists an ellipsoid that behaves like a trapping region (positively invariant set).

The natural question at this point is: is what is attracting the trajectories entering the ellipsoid for $r > r_H$? Of course it cannot be any of the fixed points since they are all unstable. How about a stable isolated *limit cycle* living within the ellipsoid?

Ruling out stable limit cycles. Lorenz came up with an ingenious heuristic approach to rule out the existence of stable limit cycles within the ellipsoidal trapping region for $r > r_H$. To this end, let us set $\sigma = 10$ and $b = 8/3$. This set of parameters yields $r_H = 24.74$. We choose $r = 28$, which is greater than r_H so that no stable fixed points exist, and plot one trajectory of the system corresponding to and arbitrary initial condition for sufficiently long time. With such trajectory available we can identify the relative maxima of the phase variable $Z(t)$ (see Figure 9) Let us call such sequence of relative maxima

$$\{z_1, z_2, z_3, \ldots\}. \tag{38}$$

Next, look for a map f that takes in one relative maximum and it returns the next one, i.e.,

$$z_{n+1} = f(z_n). \tag{39}$$

The map f is called *Lorenz's map* and it is plotted in Figure 10 using simulation data shown in Figure 9.

Period-1 orbits: A period-1 orbit, i.e. a state in which the previous relative maximum is mapped to itself, is identified by the condition

$$z^* = f(z^*), \tag{40}$$

i.e., it is a fixed point of the Lorenz map (see Figure 10). Of course if such fixed point is stable then $Z(t)$ should eventually hit the basin of attraction of such point and settle to a period-1 orbit. To study stability of z^* we investigate the dynamics of a small perturbation η_0 via the iteration

$$z^* + \eta_{n+1} = f(z^* + \eta_n) \simeq f(z^*) + f'(z^*)\eta_n. \tag{41}$$

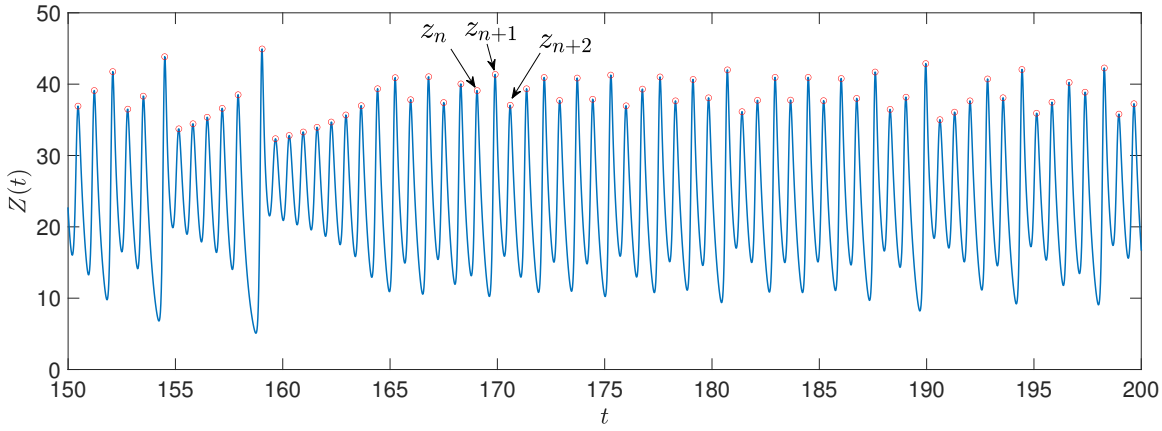

Figure 9: Trajectory of the Lorenz system (8) for $r = 28$, $\sigma = 10$ and $b = 8/3$. Shown is the phase variable $Z(t)$ and its maxima z_n. A necessary condition for the system to settle on a stable periodic orbit is that $Z(t)$ repeats itself after some finite period of time.

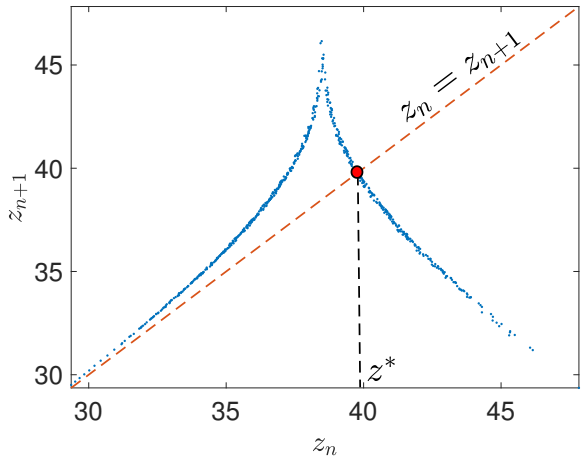

Figure 10: Lorenz's map for $r = 28$, $\sigma = 10$ and $b = 8/3$. Note that blue points are not exactly sitting on a line but rather on an very thin set.

Recalling (40), we see that the perturbation η_n satisfies

$$\eta_{n+1} = f'(z^*)\eta_n. \tag{42}$$

Taking the absolute value and iterating back to the initial perturbation yields

$$|\eta_{n+1}| = \left|f'(z^*)\right| |\eta_n| = \left|f'(z^*)\right|^2 |\eta_{n-1}| = \cdots = \left|f'(z^*)\right|^n |\eta_0| \,. \tag{43}$$

This equation shows that $|\eta_{n+1}| \to 0$ as n goes to infinity if and only if

$$\left|f'(z^*)\right| < 1. \tag{44}$$

However, the numerical results shown in Figure 10, suggest that the Lorenz map satisfies instead

$$|f'(z)| > 1 \qquad \text{for all } z. \tag{45}$$

Hence, period-1 orbits are *unstable*.

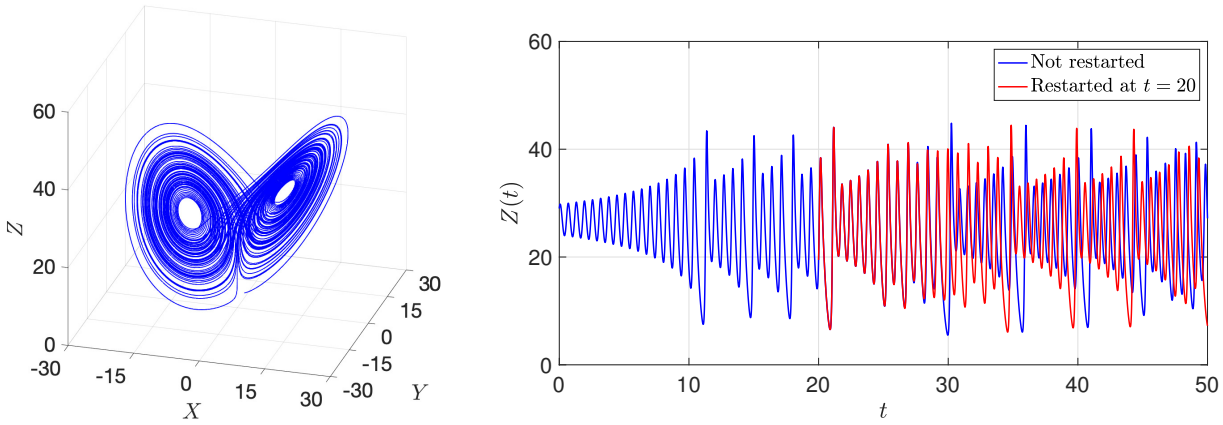

Figure 11: (a)Lorenz's attractor for $r = 28$, $\sigma = 10$ and $b = 8/3$. Shown is one orbit converging to the attractor as t increases. (b) Sensitivity to initial conditions. Integration of the Lorenz system with parameters $r = 28$, $\sigma = 10$ and $b = 8/3$ is restarted at $t = 20$ with an initial condition taken from the non-restarted simulation and rounded to three decimal digits.

Period-2 orbits: By following a similar argument it is possible to rule out stability of period-2 orbits. Such orbits define a cycle satisfying

$$z^* = f(f(z^*)). \tag{46}$$

The stability of period-2 orbits can be studied as before, by investigating how a small perturbation η_0 in a neighborhood of z^* propagates as the Lorenz map is iterated (46). We have,

$$z^* + \eta_{n+1} = f(f(z^* + \eta_n)) = f(f(z^*) + f'(z^*)\eta_n)) = f(f(z^*)) + f'(f'(z^*))f'(z^*)\eta_n, \tag{47}$$

i.e., (using (46))

$$\eta_{n+1} = f'(f'(z^*))f'(z^*)\eta_n \qquad \Rightarrow \qquad |\eta_{n+1}| = \left|f'(f'(z^*))f'(z^*)\right| |\eta_n| \,. \tag{48}$$

Hence a necessary and sufficient condition for stability of period-2 orbits is

$$\left|f'(f'(z^*))f'(z^*)\right| = \left|f'(f'(z^*))\right| \left|f'(z^*)\right| < 1, \tag{49}$$

which is impossible because of (45). Hence there are no stable period-2 orbits.

Period-p orbits: By following a similar argument it is straightforward to show that if (45) is satisfied then there are no stable period-p orbits.

In summary, there is no stable limit cycle within the ellipsoidal trapping region. What is attracting all trajectories then?

The Lorenz attractor. What actually happens to the trajectories of the Lorenz system (8) for $r = 28$ ($\sigma = 10$ and $b = 8/3$) is that they are all attracted by a "non-standard" geometric object (a *strange attractor*) with Hausdorff dimension[4] 2.0627, i.e., not a surface nor a volume but something in-between, i.e., "almost a surface". The "almost" part (and the reason why the Hausdorff dimension is not an integer) is related to the roughness of the surface, which makes it look like a fractal object. The existence of the

[4]The Hausdorff dimension is a measure of dimension that was introduced in 1918 by the mathematician Felix Hausdorff. Hausdorff dimension coincides with regular dimension of smooth objects such as surfaces (dim=2) and volumes (dim=3). The calculation of the Hausdorff dimension is usually done numerically, e.g., in the paper *"The fractal property of the Lorenz attractor"*, Physica D, vol. **190** (2004) 115–128.

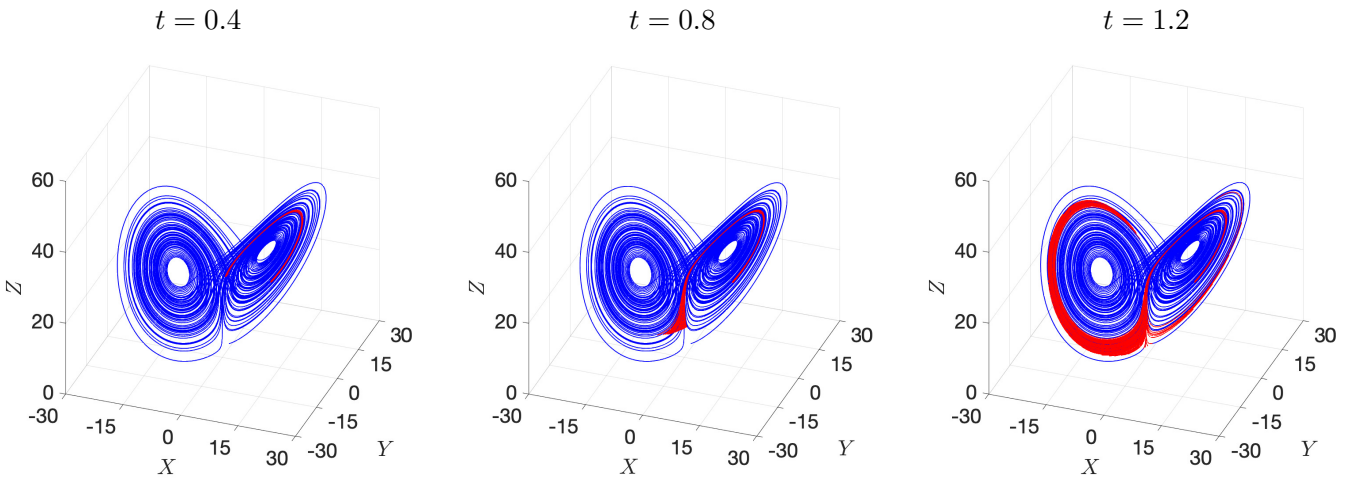

Figure 12: (a)Lorenz's attractor for $r = 28$, $\sigma = 10$ and $b = 8/3$, sensitivity to initial conditions. Shown are trajectories corresponding to a small ball of initial conditions placed nearby the attractor. As time increases such small ball of red initial conditions paints the entire attractor.

strange attractor for the Lorenz system was established in 1999 by Warwick Tucker in his PhD thesis, and in a follow-up paper titled *"The Lorenz attractor exists"* (C. R. Acad. Sci. Paris, vol. **328**, pp. 1197-1202). The proof was based on a combination of normal form theory and rigorous numerical computations. In other words, rather than producing a traditional mathematical proof, Tucker constructed an algorithm which, if successfully executed, proves the existence of the strange attractor.

The Lorenz attractor yields long-term *aperiodic behavior* of all trajectories not sitting on the Z-axis, and a high *sensitivity to initial conditions*. In Figure 12(a) we plot one trajectory of (8) for $r = 28$, $\sigma = 10$ and $b = 8/3$. It is seen that such trajectory settles to an attractor that resemble a butterfly (hence the name "butterfly attractor"). In Figure 12(b) we demonstrate what happens to a trajectory if the integration process is restarted at $t = 20$ with an initial condition taken from the non-restarted simulation and rounded to three decimal digits. The sensitivity to initial condition is also demonstrated in Figure **??**

Appendix A: Liouville's theorem

In this appendix we study how the volume of a compact region $D_0 \subset \mathbb{R}^n$ changes in time when all of its points $\boldsymbol{x}_0 \in D_0$ are advected by the flow generated by the n-dimensional dynamical system

$$\begin{cases} \dfrac{d\boldsymbol{x}}{dt} = \boldsymbol{f}(\boldsymbol{x}), \\ \boldsymbol{x}(0) = \boldsymbol{x}_0. \end{cases} \tag{50}$$

To this end, we assume that $\boldsymbol{f}(\boldsymbol{x})$ is at least continuously differentiable in $\boldsymbol{x}$m and recall that the volume of a region $D(t)$ advected by the flow generated by (50) can be expressed as (see Figure 13)

$$V(t) = \int_{D(t)} 1 d\boldsymbol{x} \tag{51}$$

where $d\boldsymbol{x} = dx_1 \cdots dx_n$. Since the flow $\boldsymbol{X}(t, \boldsymbol{x}_0)$ is invertible, we can transform the coordinates back to $\boldsymbol{x}_0$ and write the integral (51) as

$$V(t) = \int_{D_0} \det\left(\frac{\partial X(t, \boldsymbol{x}_0)}{\partial \boldsymbol{x}_0}\right) d\boldsymbol{x}_0, \tag{52}$$

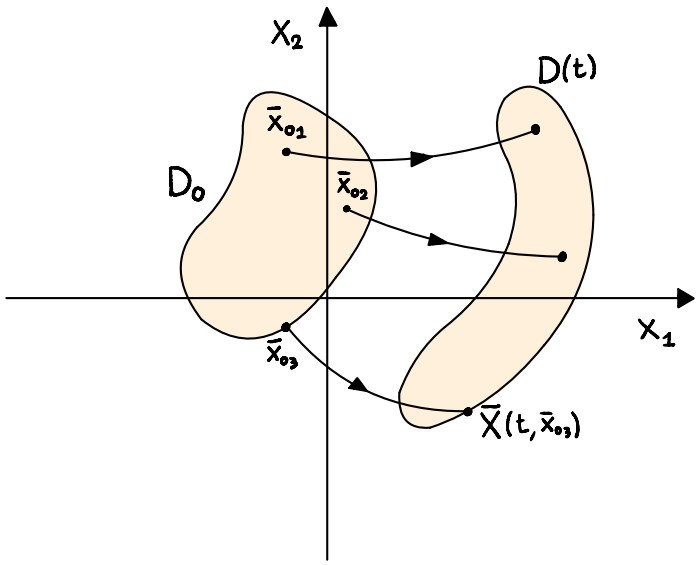

Figure 13: Sketch showing how a domain $D_0 \subset \mathbb{R}^2$ is transported to $D(t) \subset \mathbb{R}^2$ by the flow $\boldsymbol{X}(t,\boldsymbol{x}_0)$ generated by the the dynamical system (50). The rate of change in time of the volume/area of $D(t)$, i.e., $dV(t)/dt$ is given by Liouville's Theorem 2.

where

$$\det\left(\frac{\partial \boldsymbol{X}(t,\boldsymbol{x}_0)}{\partial \boldsymbol{x}_0}\right) = \det\left(\begin{bmatrix} \dfrac{\partial X_1(t,\boldsymbol{x}_0)}{\partial x_{01}} & \cdots & \dfrac{\partial X_1(t,\boldsymbol{x}_0)}{\partial x_{0n}} \\ \vdots & \ddots & \vdots \\ \dfrac{\partial X_n(t,\boldsymbol{x}_0)}{\partial x_{01}} & \cdots & \dfrac{\partial X_n(t,\boldsymbol{x}_0)}{\partial x_{0n}} \end{bmatrix}\right) \tag{53}$$

is the Jacobian determinant of the coordinate change[5] $\boldsymbol{X}(t,\boldsymbol{x}_0) \leftrightarrow \boldsymbol{x}_0$ at each time t.

Theorem 1. Let $\boldsymbol{X}(t,\boldsymbol{x}_0)$ be the flow generated by (50). Then the Jacobian determinant of $\boldsymbol{X}(t,\boldsymbol{x}_0)$, i.e., (53), satisfies

$$\frac{\partial}{\partial t}\det\left(\frac{\partial \boldsymbol{X}(t,\boldsymbol{x}_0)}{\partial \boldsymbol{x}_0}\right) = \nabla\cdot\boldsymbol{f}(\boldsymbol{X}(t,\boldsymbol{x}_0))\det\left(\frac{\partial \boldsymbol{X}(t,\boldsymbol{x}_0)}{\partial \boldsymbol{x}_0}\right). \tag{54}$$

Proof. Let us prove the theorem for two-dimensional dynamical systems. In this case, the determinant (53) can be written as

$$\det\left(\frac{\partial \boldsymbol{X}(t,\boldsymbol{x}_0)}{\partial \boldsymbol{x}_0}\right) = \frac{\partial X_1}{\partial x_{01}}\frac{\partial X_2}{\partial x_{02}} - \frac{\partial X_2}{\partial x_{01}}\frac{\partial X_1}{\partial x_{02}}. \tag{55}$$

Differentiate (55) with respect to time to t to obtain

$$\begin{aligned}\frac{\partial}{\partial t}\det\left(\frac{\partial \boldsymbol{X}(t,\boldsymbol{x}_0)}{\partial \boldsymbol{x}_0}\right) =& \frac{\partial}{\partial x_{10}}\left(\frac{dX_1(t,\boldsymbol{x}_0)}{dt}\right)\frac{\partial X_2(t,\boldsymbol{x}_0)}{\partial x_{20}} + \frac{\partial X_1(t,\boldsymbol{x}_0)}{\partial x_{10}}\frac{\partial}{\partial x_{20}}\left(\frac{dX_2(t,\boldsymbol{x}_0)}{dt}\right) - \\ & \frac{\partial}{\partial x_{20}}\left(\frac{dX_1(t,\boldsymbol{x}_0)}{dt}\right)\frac{\partial X_2(t,\boldsymbol{x}_0)}{\partial x_{10}} - \frac{\partial X_1(t,\boldsymbol{x}_0)}{\partial x_{20}}\frac{\partial}{\partial x_{10}}\left(\frac{dX_2(t,\boldsymbol{x}_0)}{dt}\right).\end{aligned} \tag{56}$$

At this point we recall that

$$\frac{dX_i(t,\boldsymbol{x}_0)}{dt} = f_i\left(X_1(t,\boldsymbol{x}_0), X_2(t,\boldsymbol{x}_0)\right), \qquad i=1,2, \tag{57}$$

[5] We know that the flow map $\boldsymbol{X}(t,\boldsymbol{x}_0)$ generated by a smooth (at least C^1) dynamical system is invertible at each point where the solution to (50) exists and is unique (see the course note 3).

which implies that

$$\begin{aligned}
\frac{\partial}{\partial x_{10}}\left(\frac{dX_1(t,\boldsymbol{x}_0)}{dt}\right) &= \frac{\partial f_1\left(X_1(t,\boldsymbol{x}_0),X_2(t,\boldsymbol{x}_0)\right)}{\partial x_{10}} = \frac{\partial f_1}{\partial x_1}\frac{\partial X_1}{\partial x_{10}} + \frac{\partial f_1}{\partial x_2}\frac{\partial X_2}{\partial x_{10}},\\
\frac{\partial}{\partial x_{20}}\left(\frac{dX_1(t,\boldsymbol{x}_0)}{dt}\right) &= \frac{\partial f_1\left(X_1(t,\boldsymbol{x}_0),X_2(t,\boldsymbol{x}_0)\right)}{\partial x_{20}} = \frac{\partial f_1}{\partial x_1}\frac{\partial X_1}{\partial x_{20}} + \frac{\partial f_1}{\partial x_2}\frac{\partial X_2}{\partial x_{20}},\\
\frac{\partial}{\partial x_{10}}\left(\frac{dX_2(t,\boldsymbol{x}_0)}{dt}\right) &= \frac{\partial f_2\left(X_1(t,\boldsymbol{x}_0),X_2(t,\boldsymbol{x}_0)\right)}{\partial x_{10}} = \frac{\partial f_2}{\partial x_1}\frac{\partial X_1}{\partial x_{10}} + \frac{\partial f_2}{\partial x_2}\frac{\partial X_2}{\partial x_{10}},\\
\frac{\partial}{\partial x_{20}}\left(\frac{dX_2(t,\boldsymbol{x}_0)}{dt}\right) &= \frac{\partial f_2\left(X_1(t,\boldsymbol{x}_0),X_2(t,\boldsymbol{x}_0)\right)}{\partial x_{20}} = \frac{\partial f_2}{\partial x_1}\frac{\partial X_1}{\partial x_{20}} + \frac{\partial f_2}{\partial x_2}\frac{\partial X_2}{\partial x_{20}}.
\end{aligned}$$

A substitution of these expressions back into (56) yields

$$\begin{aligned}
\frac{\partial}{\partial t}\det\left(\frac{\partial \boldsymbol{X}(t,\boldsymbol{x}_0)}{\partial \boldsymbol{x}_0}\right) =& \frac{\partial f_1}{\partial x_1}\frac{\partial X_1}{\partial x_{10}}\frac{\partial X_2}{\partial x_{20}} + \frac{\partial f_1}{\partial x_2}\frac{\partial X_2}{\partial x_{10}}\frac{\partial X_2}{\partial x_{20}} + \frac{\partial f_2}{\partial x_1}\frac{\partial X_1}{\partial x_{20}}\frac{\partial X_1}{\partial x_{10}} + \frac{\partial f_2}{\partial x_2}\frac{\partial X_2}{\partial x_{20}}\frac{\partial X_1}{\partial x_{10}} -\\
& \frac{\partial f_1}{\partial x_1}\frac{\partial X_1}{\partial x_{20}}\frac{\partial X_2}{\partial x_{10}} - \frac{\partial f_1}{\partial x_2}\frac{\partial X_2}{\partial x_{20}}\frac{\partial X_2}{\partial x_{10}} - \frac{\partial f_2}{\partial x_1}\frac{\partial X_1}{\partial x_{10}}\frac{\partial X_1}{\partial x_{20}} - \frac{\partial f_2}{\partial x_2}\frac{\partial X_2}{\partial x_{10}}\frac{\partial X_1}{\partial x_{20}},\\
=& \underbrace{\left(\frac{\partial f_1}{\partial x_1} + \frac{\partial f_2}{\partial x_2}\right)}_{\nabla\cdot\boldsymbol{f}}\det\left(\frac{\partial \boldsymbol{X}(t,\boldsymbol{x}_0)}{\partial \boldsymbol{x}_0}\right),
\end{aligned}$$

which proves the theorem. A similar proof can be given in n dimensions using the expression of the determinant of a $n \times n$ matrix in terms of the Levi-Civita symbol.

□

Note that at $t = 0$ we have $\boldsymbol{X}(0,\boldsymbol{x}_0) = \boldsymbol{x}_0$ and therefore

$$\det\left(\frac{\partial \boldsymbol{X}(0,\boldsymbol{x}_0)}{\partial \boldsymbol{x}_0}\right) = \det(\boldsymbol{I}) = 1. \tag{58}$$

With this initial condition it is immediate to integrate the (separable) ODE (54) to obtain

$$\det\left(\frac{\partial \boldsymbol{X}(t,\boldsymbol{x}_0)}{\partial \boldsymbol{x}_0}\right) = \exp\left[\int_0^t \nabla\cdot\boldsymbol{f}(\boldsymbol{X}(\tau,\boldsymbol{x}_0))d\tau\right] \tag{59}$$

We now have all element to prove the following theorem due to Liouville.

Theorem 2 (Liouville's theorem)**.** The volume $V(t)$ of a compact region $D(t) \subset \mathbb{R}^n$ advected by the flow $\boldsymbol{X}(t,\boldsymbol{x}_0)$ generated by a smooth dynamical system of the form (50) satisfies

$$\frac{dV(t)}{dt} = \int_{D(t)} \nabla\cdot\boldsymbol{f}(\boldsymbol{x})d\boldsymbol{x} \tag{60}$$

Proof. The volume of $D(t)$ can be expressed as (see equation (52))

$$V(t) = \int_{D_0} \det\left(\frac{\partial X(t,\boldsymbol{x}_0)}{\partial \boldsymbol{x}_0}\right) d\boldsymbol{x}_0 \tag{61}$$

Differentiating with respect to time and using (54) yields

$$\begin{aligned}\frac{dV(t)}{dt} =& \frac{\partial}{\partial t}\int_{D_0} \det\left(\frac{\partial X(t,\boldsymbol{x}_0)}{\partial \boldsymbol{x}_0}\right) d\boldsymbol{x}_0 \\ =& \int_{D_0} \frac{\partial}{\partial t} \det\left(\frac{\partial X(t,\boldsymbol{x}_0)}{\partial \boldsymbol{x}_0}\right) d\boldsymbol{x}_0 \\ =& \int_{D_0} \nabla\cdot\boldsymbol{f}\left(\boldsymbol{X}(t,\boldsymbol{x}_0)\right) \det\left(\frac{\partial X(t,\boldsymbol{x}_0)}{\partial \boldsymbol{x}_0}\right) d\boldsymbol{x}_0 \\ =& \int_{D(t)} \nabla\cdot\boldsymbol{f}\left(\boldsymbol{x}\right) d\boldsymbol{x}. \end{aligned} \tag{62}$$

□